Design of a Resonant Point-Multipoint Wireless Power Transmission System

Úrsula C. Resende, Thiago H. G. Mello
Department of Electrical Engineering, CEFET-MG, Minas Gerais 30510-000, Brazil

***Abstract*—With the exponential growth of IoT (Internet of Things), Industry 4.0, and electrical vehicles, there is a growing need for flexible energy sources. Wireless energy transfer is becoming increasingly important in this context, as it enables physical devices to be more flexible and allows for the simultaneous powering of multiple loads. This study presents a wireless energy transfer system that uses solenoid coils in inductive resonant mode. The system is configured in a point-multipoint setup, with a circular transmitter coil and two identical circular receiver coils placed inside the transmitter. We use mathematical modeling to develop circuit theory models and identify the most efficient topology for the system. In addition, we propose a simple and cost-effective self-oscillating electronic converter design with two switches for system supply. Our numerical and experimental results demonstrate that the proposed system is viable and functional, achieving a power output of 1.7 W and efficiency of 27%.**

***Index Terms*—Point-Multipoint, Resonance, Self-Oscillating Inverter, Wireless Power Transmission.**

I. Introduction

THERE has been a long time since the scientific community has investigated different apparatus to perform wireless power transmission (WPT). This discussion is mainly motivated by the growing demand for portable, miniaturized, and low-cost electronic devices that enables the development of contemporary technological paradigms such as the Internet of Things (IoT), Industry 4.0, and electrical vehicles. Therefore, the constraints on economy, mobility, and accessibility are crucial to developing newer WPT solutions.

The WPT techniques in electrical engineering can be classified into three main categories: near-field, far-field, and optical [1], [2]. Near-field techniques utilize inductive coupling (IC) or resonant inductive coupling (RIC), while far-field techniques rely on propagating waves in the microwave range. On the other hand, optical techniques utilize laser technologies.

IC systems operate by inducing current through an alternating magnetic flux generated by the transmitter unit, similar to transformers. These systems are simple but suffer from low power transfer due to poor coupling between the transmitter and receiver coils. As a result, the transmitter and receiver units must be placed in close proximity and perfectly aligned.

In contrast, RIC systems utilize resonant coupling, where the coils operate at the same resonant frequency and are strongly coupled. This allows for efficient power transfer over larger distances. The resonant frequency can be adjusted by incorporating external capacitors. RIC techniques have gained significance in the development of efficient wireless transmission systems, finding applications in various areas such as vehicles [3] and mobile device chargers [4], healthcare [5], surgical robots [6], [7], and more [8]–[10].

The application of RIC configurations in multi-point systems has gained attention in recent years to meet the increasing demand for simultaneous power delivery to multiple loads [11], [12]. However, compared to single-point transmission, this area remains relatively unexplored. Another crucial aspect is the choice of an appropriate electronic converter for powering the system. While microcontroller units are commonly search, their use can escalate project complexity and expenses. Thus, the challenge lies in developing an efficient and cost-effective device that operates at the system design frequency while delivering the desired power output.

The main contribution of this work is to comprehensively design a point-multipoint RIC system, consisting of a solenoid transmitter coil and two identical solenoid receiver coils positioned side by side on the same plane as the transmitter coil, thus characterizing a point-multipoint system. The objective is to investigate the configuration that achieves the highest efficiency and output power in systems with multiple and strong magnetic coupling. Moreover, an appropriate design of a self-oscillating electronic converter for power supply is presented. The self-oscillating configuration is chosen for its construction simplicity and cost-effectiveness, although it requires precise design and tuning to match the system's operating frequency. Numerical and experimental results are then compared to demonstrate the feasibility and functionality of the proposed system.

II. System Description

The system consists of three coil units: one transmitter unit (TU) and two identical receiver units (RUs). The coils parameters were defined to ensure a planar assembly that can be inserted into, for example, a personal office table to wirelessly charge multiple devices. Therefore, the system and electronic converter proposed were designed to supply a total power output of approximately 5 W, which is sufficient for powering small electronic devices. Additionally, the converter was designed to be powered by a commercially available 14 V DC source.

A. Resonance Condition and Operation Frequency

By carefully selecting external capacitors, known as compensation capacitors, and connecting them to the coils, the resonance condition can be achieved. This condition ensures that the inductive and capacitive reactances have equal

magnitudes, resulting in a purely resistive impedance. The resonance frequency, f_r, then corresponds to the desired operating frequency of the system. The choice of connecting the capacitors in series or parallel with the coils depends on various parameters, such as mutual inductance and the converter topology employed. This deliberate configuration of the compensation capacitors enhances the efficiency and extends the transmission distance range of the RIC system.

For the proposed system, the operating frequency (f) range is 650 kHz to 1.2 MHz. This range was chosen based on factors such as the cost and availability of electronic converter switches (MOSFETs), losses due to skin effect, the size of the assembly, and the expected transmission distance, which decreases as f increases. It is worth noting that this frequency range enables accurate mathematical modeling using circuit theory, as the wavelength of the traveling signal is significantly longer than the system dimensions.

B. Coils Design and Placement

Wireless powering systems based on RIC operate through magnetic field coupling in the near field region. Therefore, the coils must be positioned within this limit which is directly related to the operating frequency [13]. Each unit in the system consists of a wire main coil and a wire auxiliary guide coil known as the "drive" coil. The TU is composed of coils B_1 (drive) and B_2 (main) while RUs consist of coils B_3 (main) and B_4 (drive), as illustrated in Fig. 1.(a). The RUs are placed inside the TU, forming a planar network, as depicted in Figs. 1.(a) and (b). It is important to note that there exists a lateral displacement of 6.2 cm between the centers of the TU and the RUs. All main coils and their respective drive coils are concentric, and the RUs are symmetrically positioned with respect to the TU.

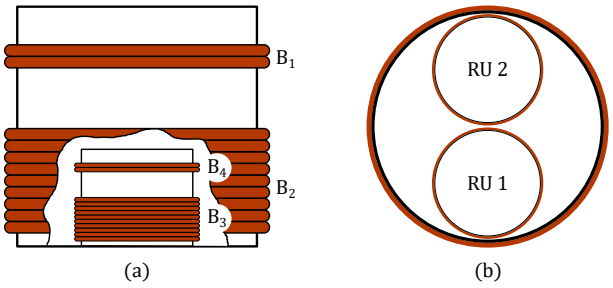

Fig. 1. WPT multipoint planar system. (a) side view and (b) top view. B_1 is the transmitter drive coil, B_2 is the transmitter main coil, B_3 is the receiver main coil and B_4 is the receiver drive coil.

The design of the coils involves several parameters, including the number of turns (NT), coil radius (CR), spacing between drive and main coils, and the wire gauge (WG). These parameters, along with the geometry, determine important electrical characteristics such as self-inductance (L), mutual inductance (M), and resistance (R). To achieve a desired flat shape with a high inductance-to-resistance ratio, which results in a higher quality factor, we opted for a reduced number of turns: 2 turns for the drives, 10 turns for the receiver main coils, and 9 turns for the transmitter main coil. Additionally, these coils were designed without any spacing between them. The specific parameter values for each coil can be found in Table I.

TABLE I
COIL PARAMETERS

Coil	NT	WG (mm)	CR (m)
Drive TU	2	1.35	0.13
Drive RUs	2	0.5	0.053
Main TU	9	1.35	0.13
Main RUs	10	0.5	0.053

The decision to use a reduced number of turns for the coils was made to mitigate the impact of strongly coupled phenomena such as splitting [14], [15] and cross-coupling [16], [17], which are closely related to the system's mutual inductance. While this choice may limit the achievable quality factor, it helps improve the overall transmission performance, particularly in cases where the coils are positioned in close proximity to each other. By minimizing these effects, we can enhance the efficiency and reliability of the wireless power transfer system.

III. SYSTEM MODELING

Once the system topology is defined, the mathematical modeling of the coil resistance, self-inductance, and mutual inductance is carried out.

A. Ohmic Resistance

To calculate the coil ohmic resistance (R_Ω), the skin effect must be considered in alternated circuits (AC), which causes the current tendency to be concentrated near the conductor's boundary. Thus, the effective area of the material in which electrons flow is reduced, increasing the R_Ω value. Therefore, R_Ω can be calculated in this case by [13]

$$R_\Omega = \frac{\alpha N}{\sigma r_c \delta}, \tag{1}$$

where α is the average coil radius, σ is the material conductivity, r_c is the conductor radius, N is the number of turns, and δ is the penetration depth given by $1/\sqrt{\pi f \mu \sigma}$ with μ being the magnetic permeability of the medium.

The presence of a radiation resistance (R_r) is typically associated with AC circuits. However, in our case, the operating frequency f is relatively low, and as a result, the impact of R_r can be considered negligible compared to R_Ω. Thus, we can assume that R_Ω dominates the overall resistance R in the system, and the contribution of R_r can be disregarded.

B. Self-Inductance

Over the years, various approximate equations have been developed to calculate coil inductance due to the computational complexity of rigorous numerical solutions. One commonly used approach is based on the assumption that the self-inductance L of a coil, where the diameter (D) is much smaller than its height (l) ($D \ll l$), can be approximated

by considering overlapping infinite conductors of infinitesimal thickness without electrical contact [18]. This approach, known as the current sheet approximation, also provides a correction coefficient that can be applied when the coil radius ($r = D/2$) becomes comparable to its height ($r \approx l$) [19]. The approach established by this model is [19]

$$L = \frac{\mu\pi r^2 N^2 k_L}{l}, \tag{2}$$

where r and N are the radii and number of turns, respectively. The Nagaoka correction coefficient k_L is defined as [19]

$$k_L = \frac{4(D/L)}{3\pi}\left[\frac{(2\kappa^2-1)}{\kappa^3}E(\kappa) + \frac{1-\kappa^2}{\kappa^3}K(\kappa) - 1\right]. \tag{3}$$

$K(\kappa)$ and $E(\kappa)$ are the first and the second elliptic integrals, respectively, and κ, integral module, is [19]:

$$\kappa = \sin\theta = \frac{D}{\sqrt{D^2 + l^2}}, \tag{4}$$

with θ and all the others coil parameters being illustrated in Fig. 2.

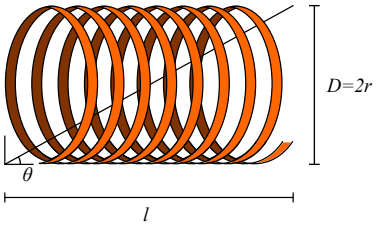

Fig. 2. Current sheet solenoid.

C. Mutual Inductance

Mutual inductance M between two current sheets can be calculated by using the modeling presented in [20], which approximates mutual inductance between two parallel closed paths displaced laterally by

$$M = \frac{\mu ab}{\sqrt{a(b+\Delta)}}G(\rho_{máx}), \tag{5}$$

where a and b are the radii of the two turns, Δ is the lateral misalignment, and $\rho_{máx}$ is:

$$\rho_{máx} \equiv \sqrt{\frac{4a(b+\Delta)}{(a+b+\Delta)^2 + d^2}}, \tag{6}$$

where d represents the vertical distance between coils. In (5), $G(\rho)$ is calculated from:

$$G(\rho) = \left(\frac{2}{\rho} - \rho\right)K(\rho) - \frac{2}{\rho}E(\rho), \tag{7}$$

where ρ is the distance between the point of the infinitesimal length element of the integrated loop and the center of the other loop. All parameters presented from (5) to (7) can be identified in Fig. 3.

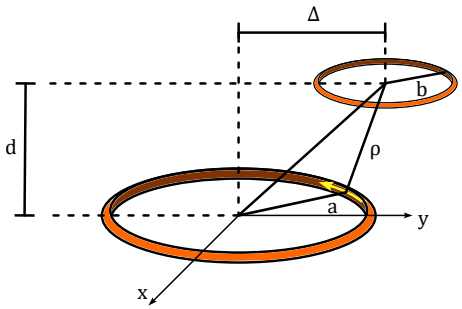

Fig. 3. Parameters for the mutual inductance calculation between loops with side and vertical misalignment.

Although there are other equations for misalignment in the literature, (5) was the one that best fit physical problem conditions ($\Delta > b$) [20]. For coils i and j with n_i and n_j turns, respectively:

$$M_{ij} = \sum_{k=1}^{n_i}\sum_{l=1}^{n_j} M_{kl} \tag{8}$$

D. Point-Multipoint System

To mathematically model the proposed RIC structure, the mesh current theorem and the voltage Kirchhoff's law in the phasor domain are utilized. Fig. 4 illustrates the circuit models for the two investigated RIC system configurations. The drive coils are connected to the power source and system loads, while the main coils, responsible for the RIC between TU and RU, are placed in series with the compensation capacitor. The transmitter drive coil is fully compensated in parallel, as required by the chosen self-oscillating electronic converter topology. The performance of the receiver drive coils is studied for both series and parallel connections of the external capacitor. In the circuit diagrams, R_{L1} and R_{L2} represent the resistive loads connected to the terminals of the receiver drive coils, R denotes the equivalent coil resistance, V_s represents the power source, C is the external compensation capacitor, and L represents the coil self-inductance. The indexes 1 to 6 indicate the corresponding circuit parameters. For this study, resistive loads of 10 Ω were chosen.

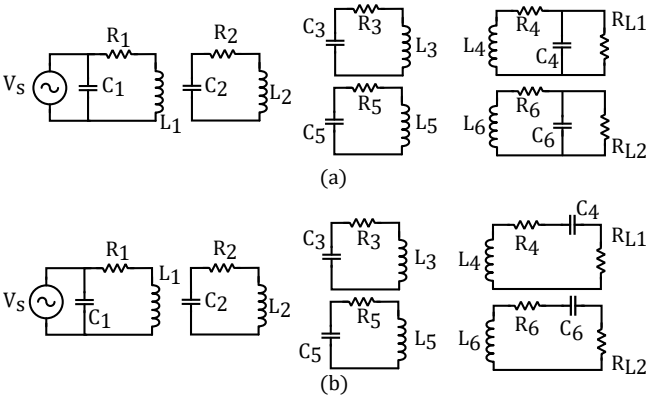

Fig. 4. Point-multipoint systems. (a) Parallel-parallel (PP) and (b) parallel-series (PS) compensations.

IV. Self-Oscillating Electronic Converter

The operating frequency range of 650 kHz to 1.2 MHz was selected considering the availability and cost of commercially available electronic switches, as well as the physical dimensions of the proposed system. To ensure operational efficiency, the chosen electronic converter topology must satisfy specific requirements. Among the various power converter topologies, the class D topology is deemed most suitable due to its low switch stress and capability to deliver medium to high output power levels [21]–[23]. However, such devices often employ pulse modulation for switch activation, thereby increasing project complexity and cost. Hence, a self-oscillating converter was selected to power the proposed RIC system in this study. Self-oscillating configurations offer the benefit of automatic switching command execution and adjusting f to match the specific f_r. Additionally, they eliminate the need for digital signal processing in feedback control loops, thereby reducing cost and complexity. To model, design, and simulate the converter, the software Multisim® was employed. This software enables consideration of real parameters of electronic components (using SPICE models) and facilitates time domain simulations.

To operate within the selected frequency range and achieve maximum output power, a specific topology was chosen, as depicted in Fig. 5. This topology utilizes a transmitter drive coil as a tank circuit and requires parallel compensation [24]. In the circuit, R_{p1} and R_{p2} represent polarization resistors for the 100 Ω switches, R_1 and R_2 are resistances added to the 5 μH radio frequency choke (RFC) inductors (L_{osc1} and L_{osc2}), $D1$ and $D2$ are fast recovery feedback loop diodes (1N4148), Q_1 and Q_2 are active switching elements (IRF540 MOSFETs), V_{cc} is a 14 V DC source, and C_1, R_1, and L_1 represent the external compensation capacitor, equivalent series resistance, and self-inductance of the tank circuit, respectively. The values for non-tank components were determined empirically to ensure proper voltage and current levels within the limits of the active components, while also achieving the desired output signal level across L_1. During converter operation, when one of the switches Q is closed, the other is opened due to the feedback diodes. Consequently, the Thèvenin equivalent circuit seen by the tank circuit (transmitter drive coil) is an alternating voltage source in series with R_1 and L_{osc1}.

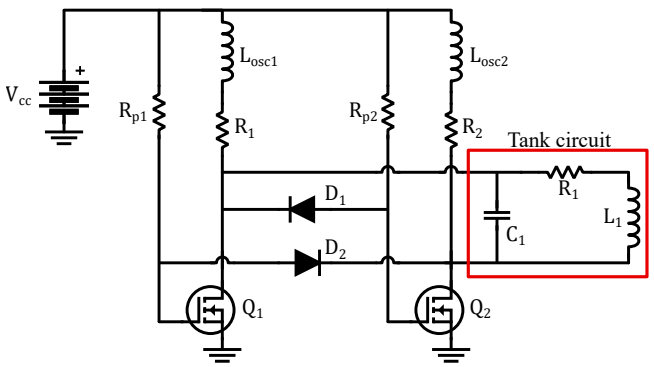

Fig. 5. Proposed self-oscillating electronic converter circuit.

V. Simulations

The mathematical modeling described in Section III was implemented in the MATLAB® environment. Simulations were conducted to evaluate the performance of the system with parallel-parallel (PP) and parallel-series (PS) compensation, taking into account the mutual inductance between all pairs of coils. The obtained results were compared and complemented with simulations performed in Multisim®, which supports real electronic component models. The Multisim® simulations encompass not only the coils and compensation capacitors but also the electronic converter, providing a more comprehensive representation of the system.

In terms of efficiency, the series-series (SS) compensation topology is the best when considering only two coils because it eliminates the reflection of the reactive portion between them [25]. However, in systems with a larger number of coils that interact magnetically or are positioned closely, the reflection of reactive components occurs even when the system is SS compensated. As a result, this phenomenon leads to a shift in f_r of the complete system compared to the resonance frequency of the individual coils. Thus, to determine the optimal arrangement of capacitors for the proposed RIC system, two simulations were conducted: 1) series compensation and 2) parallel compensation for the receiver coils, as depicted in Fig. 4. For the main coils, the only feasible connection is in series. The compensation capacitors (C) were calculated to ensure that f_r of each coil's circuit was close to 1 MHz. The values listed in Table II represent the commercially available values that are closest to the calculated ones.

TABLE II
Coil's Compensation Capacitors

Coil	Capacitance (nF)
Drive TU	9.3
Drive RUs	22
Main TU	0.68
Mains RUs	1.33

In the MATLAB® simulation, the peak-to-peak value of V_s was set to 42 V, based on the Thèvenin's voltage obtained from the Multisim® simulation. This value was chosen to achieve a total output power of at least 5 W over 10 Ω loads with a V_{cc} of 14 V. The simulation results, depicted in Fig. 6 for transmission efficiency and Fig. 7 for transmitted power, are highlighted with red dots at 1 MHz. These results correspond to the simulation of coils supplied by an AC source, without considering the electronic converter. The yellow dots represent the results obtained from simulations performed in Multisim® at the frequency where the system output became stable.

In Fig. 6, it can be observed that at the chosen operating frequency of 1 MHz, the parallel-parallel (PP) configuration achieves approximately 96% efficiency, while the parallel-series (PS) configuration achieves approximately 94%. Additionally, the PP configuration shows a steeper efficiency drop from 1.75 MHz. Beyond this frequency, the power transferred to the loads becomes negligible, rendering this frequency range

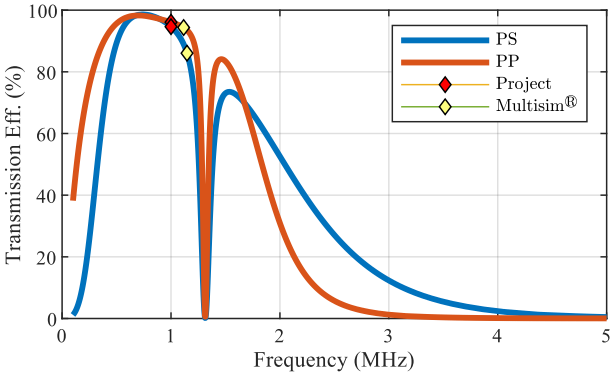

Fig. 6. Transmission efficiency (considering two loads) for PS and PP compensations (MATLAB® simulation).

unsuitable for the intended objectives. It is also evident that there is a significant efficiency dip at around 1.3 MHz due to intense constructive and destructive cross-coupling between the mutual inductances, resulting in a significant frequency splitting.

Fig. 7 demonstrates the difference in total output power at 1 MHz, with 5.6 W for the PP configuration and 3.8 W for the PS configuration. This discrepancy can be attributed to the more significant resonance frequency shift observed in the PS configuration. The results obtained for both configurations indicate that within a wide frequency range (approximately from 0.6 MHz to 1.2 MHz), high efficiency and power values can be achieved, indicating a resonant system.

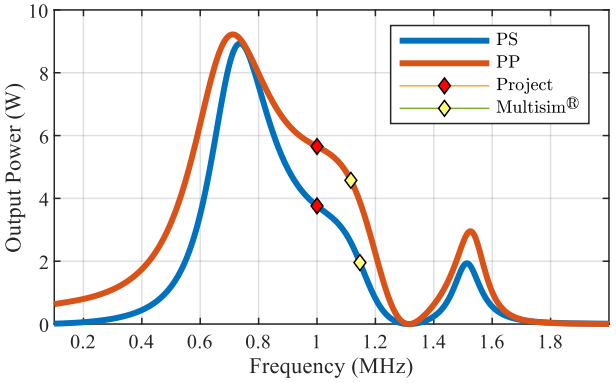

Fig. 7. Total output power (considering two loads) for PS and PP compensations (MATLAB® simulation).

The variation between the Multisim® results (yellow marks) and the MATLAB® results is due to the ideal AC source used in the MATLAB® simulation, as opposed to the real model of the electronic converter.

During the Multisim® simulation, it was observed that using V_{cc} values lower than 6 V resulted in unstable behavior of the electronic converter. This finding establishes a minimum excitation value that should be considered. The load voltage ($V_{R_{L1}} = V_{R_{L2}}$) results are depicted in Fig. 8, and the performance parameters are summarized in Table III. It is worth noting that the type of system configuration directly affects the stabilizing process of the electronic converter, as it adjusts itself accordingly. As a result, the parallel-series (PS) configuration stabilizes at a higher frequency, leading to a significant reduction in the amplitude of the load voltage.

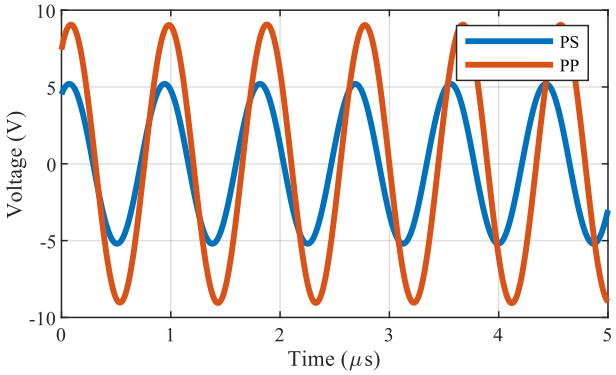

Fig. 8. Load voltage for PS and PP compensations (Multisim® simulation).

TABLE III
MULTISIM® COMPLETE SYSTEM SIMULATION PERFORMANCE

Parameter	PS	PP
Operation frequency (MHz)	1.147	1.115
Transmission eff. (without oscillator) (%)	87.1	94.7
Power per load (W)	1.4	4.1
Converter input power (W)	6.8	14.5

Based on the data presented, the PP configuration was chosen as it yielded the best results for an operating frequency close to 1 MHz, demonstrating higher efficiency and transmitted power. Although the overall system operating frequency is not equal to the resonance frequency of the individual coils, it falls within the range of good system performance.

VI. EXPERIMENTAL RESULTS

The PP system prototype underwent experimental analysis with the main objective of measuring the power delivered to the loads, as well as the transmission and overall efficiency. In order to achieve this objective, the system was tested in two ways: first, by analyzing the individual parts separately, and then by evaluating the system as a whole.

A. Electronic Converter

The Multisim® simulation results indicated that the currents flowing through L_{osc1} and L_{osc2} are approximately 1 A. In consideration of cost and the availability of components that can support this current value, the inductor construction process was chosen. An air core structure with a radius of 14 mm, 12 turns, and a wire diameter of 1 mm was designed, which allows for a significant magnetic flux density. However, this high flux density also increases the magnetic coupling with other areas of the circuit, particularly with other inductors. To mitigate this issue and maintain a compact PCB size, L_{osc1} and L_{osc2} were positioned perpendicular to each other to reduce mutual inductance. The prototype PCB layout and the assembled topology are depicted in Fig. 9.

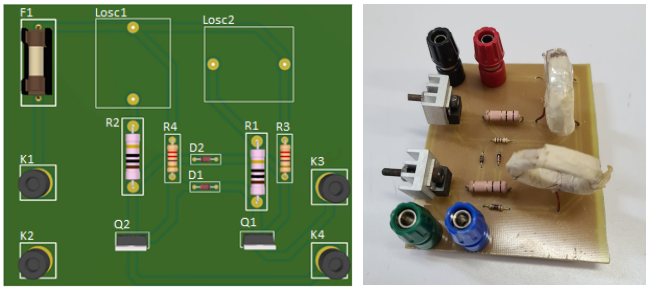

(a) (b)

Fig. 9. (a) PCB layout, and (b) real assembled prototype.

B. Circuit Parameters

A comparison was conducted between the calculated and measured inductance values to validate the proposed mathematical modeling. However, measurements of inductance values between coils in different units were not performed due to the limited power capacity of the measuring instruments. Table IV presents a comparison between the measured and simulated inductance values for the TU, RU, and the inductors in the electronic converter. The results confirm the accuracy of the proposed modeling approach, highlighting its significance as a valuable tool for the design of wireless power transmission systems.

TABLE IV
COMPARISON BETWEEN MEASURED AND SIMULATED INDUCTANCE VALUES

Parameter	Measured (μH)	Simulated (μH)	Error (%)
L_{osc1}	5.266	5	5.3
L_{osc2}	5.283	5	5.7
L_1	2.730	2.723	0.3
L_2	39.650	38.936	1.8
L_3	21.449	19.997	7.3
L_4	1.100	1.155	4.8
M_{12}	5.090	5.348	4.8
M_{34}	2.620	2.261	15.9

C. Measurements and Analysis

The power delivered by the RIC system was determined using the measured voltage over the 10 Ω loads. The total power P_{total} is calculated as follows:

$$P_{\text{total}} = \frac{V_{\text{RMS1}}^2}{R_{\text{L1}}} + \frac{V_{\text{RMS2}}^2}{R_{\text{L2}}} \tag{9}$$

Here, V_{RMSn} represents the root mean square (RMS) voltage measured on the R_{Ln} load, with $n = 1, 2$. The instantaneous voltage measured in both loads is shown in Fig. 10. From the measurements, an average RMS value of 4.15 V is observed, resulting in a delivered power of 1.72 W per load. The harmonic distortion rate (THD), considering the first six harmonics, is -41.8 dB (0.81 % THD). Spectral evaluation reveals that the fundamental harmonic is at 966 kHz, indicating a 3.4 % deviation from the project's intended operating frequency of 1 MHz.

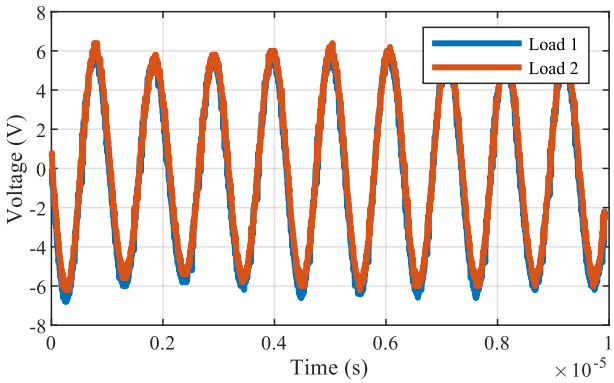

Fig. 10. RUs loads measured voltages.

In addition to the RUs, the output voltage of the electronic converter was also measured. The resulting measurement is shown in Fig. 11. The total harmonic distortion (THD) for the electronic converter output voltage is -23.8 dB (6.5 % THD), with an RMS value of 25.95 V.

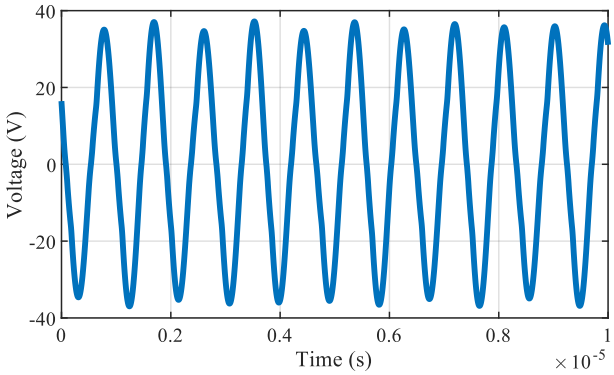

Fig. 11. Measured electronic converter output voltage.

D. Global Efficiency

Based on simulations performed in Multisim® with the measured circuit parameters, the power provided by the V_{cc} source was 11.81 W, with an average of 3.12 W delivered to each load. Therefore, the overall efficiency is 52.8 %. However, if the equivalent series resistances (ESR) of the capacitors are taken into account, considering commercial values, the output power decreases to 1.64 W for each load, with 9.96 W from the V_{cc} source. This results in an global efficiency of 32.9 %. This analysis was performed considering an operating frequency of 1.13 MHz, the frequency at which the system stabilizes.

In the MATLAB® environment, the global efficiency was measured to be 40.1 % when considering only the current fundamental harmonic and all circuit parameters being modeled without equivalent series resistances (ESR) at a frequency of 966 kHz. However, when harmonics are taken into account, the efficiency tends to decrease as the inductive circuit acts as a low-pass filter. The measured global efficiency was found to

be 27.3 % in this case, with a current of 0.9 A and a voltage of 14 V read from the DC source display, and an average of 1.72 W delivered to each load. The presence of ESR affects the cancellation of reactance between the inductor and parallel capacitor, and a significant portion of resistance is reflected back to the transmitter drive due to high mutual inductance between the coils, thereby degrading impedance matching. To achieve more efficient results, it is recommended to use low ESR capacitors.

VII. Conclusion

This work presents a point-multipoint system for wireless energy transfer using wire coils in inductive resonant mode. Both numerical and experimental results demonstrate that the proposed flat layout can serve as a charging surface for small electronic devices. The achieved global efficiency, which includes the efficiency of the electronic converter, highlights the potential of the proposed system. The close agreement between the numerical and experimental results validates the accuracy of the mathematical modeling and the reliability of the experimental methodology employed.

The robustness of the parallel-parallel configuration is confirmed, particularly in systems where the transmitter and receiver units are in close proximity, and the effects of mutual inductance are significant. The proposed self-oscillating converter topology is simple, cost-effective, and capable of operating within the intended frequency range while delivering the targeted power levels. It is important to consider a wide frequency range during system design to account for the proximity effects between the coils, which can lead to a deviation in the overall operating frequency compared to the resonant frequency of individual coils. This approach facilitates tuning of all system components. Overall, this research demonstrates the feasibility and effectiveness of the proposed wireless energy transfer system, paving the way for its practical implementation in various applications.

Acknowledgment

This work was partially supported by FAPEMIG, CAPES, Cnpq, and CEFET-MG.

References

[1] L. Xie, Y. Shi, Y. T. Hou, and A. Lou, "Wireless power transfer and applications to sensor networks," *IEEE Wireless Communications*, vol. 20, no. 4, pp. 140–145, 2013.

[2] Y. Wang, J. Qiao, J. Du, F. Wang, and W. Zhang, "A view of research on wireless power transmission," in *Journal of Physics: Conference Series*, vol. 1074, no. 1. IOP Publishing, 2018, p. 012140.

[3] A. Mahesh, B. Chokkalingam, and L. Mihet-Popa, "Inductive wireless power transfer charging for electric vehicles–a review," *IEEE Access*, vol. 9, pp. 137 667–137 713, 2021.

[4] S. Malebary, "Wireless mobile charger excursion optimization algorithm in wireless rechargeable sensor networks," *IEEE Sensors Journal*, vol. 20, no. 22, pp. 13 842–13 848, 2020.

[5] S. R. Khan, S. K. Pavuluri, G. Cummins, and M. P. Desmulliez, "Wireless power transfer techniques for implantable medical devices: A review," *Sensors*, vol. 20, no. 12, p. 3487, 2020.

[6] H. Zhuang, W. Wang, K. Zhao, Q. Fei, and G. Yan, "Design and analysis of a wireless power transfer system for capsule robot using an optimised planar square spiral transmitting coil pair," *The International Journal of Medical Robotics and Computer Assisted Surgery*, vol. 18, no. 4, p. e2399, 2022.

[7] M. Nica, C. Forbrigger, and E. Diller, "A novel magnetic transmission for powerful miniature surgical robots," *IEEE/ASME Transactions on Mechatronics*, vol. 27, no. 6, pp. 5541–5550, 2022.

[8] F. H. Sumi, L. Dutta, and F. Sarker, "Future with wireless power transfer technology," *J. Electr. Electron. Syst*, vol. 7, no. 1000279, pp. 2332–0796, 2018.

[9] A. Kurs, A. Karalis, R. Moffatt, J. D. Joannopoulos, P. Fisher, and M. Soljacic, "Wireless power transfer via strongly coupled magnetic resonances," *science*, vol. 317, no. 5834, pp. 83–86, 2007.

[10] J. Chen, C. W. Yu, and W. Ouyang, "Efficient wireless charging pad deployment in wireless rechargeable sensor networks," *IEEE Access*, vol. 8, pp. 39 056–39 077, 2020.

[11] J.-H. Cho, S. Jung, and Y.-J. Kim, "Wireless power transfer for variable load, distance, and power division ratio in a loosely-coupled multiple-receiver relay system," *IEEE Transactions on Industrial Electronics*, vol. 70, no. 7, pp. 6809–6818, 2023.

[12] C. Cheng, Z. Zhou, W. Li, C. Zhu, Z. Deng, and C. C. Mi, "A multi-load wireless power transfer system with series-parallel-series compensation," *IEEE Transactions on Power Electronics*, vol. 34, no. 8, pp. 7126–7130, 2019.

[13] M. N. O. Sadiku, *Elements of electromagnetics*. Oxford University Press, 2018.

[14] X. Liu, X. Yuan, C. Xia, and X. Wu, "Analysis and utilization of the frequency splitting phenomenon in wireless power transfer systems," *IEEE Transactions on Power Electronics*, vol. 36, no. 4, pp. 3840–3851, 2021.

[15] Z.-J. Liao, S. Ma, Q.-K. Feng, C. Xia, and D. Yu, "Frequency splitting elimination and utilization in magnetic coupling wireless power transfer systems," *IEEE Transactions on Circuits and Systems I: Regular Papers*, vol. 68, no. 2, pp. 929–939, 2021.

[16] M. Ishihara, K. Fujiki, K. Umetani, and E. Hiraki, "Automatic active compensation method of cross-coupling in multiple-receiver resonant inductive coupling wireless power transfer systems," in *2019 IEEE Energy Conversion Congress and Exposition (ECCE)*, 2019, pp. 4584–4591.

[17] P. Jayathurathnage, Y. Liu, and J. Kyyrä, "Self-decoupled and integrated coils for modular multitransmitter wireless power transfer systems," *IEEE Transactions on Power Electronics*, vol. 37, no. 11, pp. 12 962–12 967, 2022.

[18] A. C. de Queiroz, "Cálculo de indutâncias e indutâncias mútuas pelo método de maxwell," *1a. Semana da Eletrônica, UFRJ*, 2003.

[19] D. W. Knight, "An introduction to the art of solenoid inductance calculation with emphasis on radio-frequency applications," *ver. 0.20, Feb*, vol. 4, 2016.

[20] M. Soma, D. C. Galbraith, and R. L. White, "Radio-frequency coils in implantable devices: Misalignment analysis and design procedure," *IEEE Transactions on Biomedical Engineering*, vol. BME-34, no. 4, pp. 276–282, 1987.

[21] C. Jiang, K. Chau, C. Liu, and C. H. Lee, "An overview of resonant circuits for wireless power transfer," *Energies*, vol. 10, no. 7, p. 894, 2017.

[22] X. Ge, L. Cheng, Y. Yao, and W.-H. Ki, "A 6.78 mhz single-stage wireless power transmitter using a 3-mode zero-voltage switching class-d pa," *IEEE Transactions on Circuits and Systems I: Regular Papers*, vol. 68, no. 6, pp. 2736–2748, 2021.

[23] H. Kennedy, R. Bodnar, T. Lee, and W. Redman-White, "A self-tuning resonant-inductive-link transmit driver using quadrature symmetric delay trimmable phase-switched fractional capacitance," *IEEE Journal of Solid-State Circuits*, vol. 53, no. 6, pp. 1694–1706, 2018.

[24] L. Pereira, U. Resende, S. Gonçalves, M. M. Afonso, C. Vollaire, and P. Pereira, "Design of a resonant wireless power transmission system using printed inductors," in *ISEF*, 2015.

[25] K. N. Mude and K. Aditya, "Comprehensive review and analysis of two-element resonant compensation topologies for wireless inductive power transfer systems," *Chinese Journal of Electrical Engineering*, vol. 5, no. 2, pp. 14–31, 2019.